Catal Lett (2016) 146:452–463
DOI 10.1007/s10562-015-1651-z

Electrochemically Synthesized Pt/Al_2O_3 Oxidation Catalysts

Dmitry E. Doronkin[1,2] · Aleksandra B. Kuriganova[3] · Igor N. Leontyev[4] · Sina Baier[2] · Henning Lichtenberg[1,2] · Nina V. Smirnova[3,5] · Jan-Dierk Grunwaldt[1,2]

Received: 11 September 2015 / Accepted: 2 November 2015 / Published online: 20 November 2015

Abstract $Pt/\gamma–Al_2O_3$ catalysts made by fast and simple electrochemical dispersion method were characterized using X-ray absorption spectroscopy, CO chemisorption, transmission electron microscopy and X-ray diffraction, and compared with an impregnated catalyst with respect to oxidation of CO and NO. A combination of techniques revealed average particle sizes of 3–4 nm for 0.81–3.8 wt% $Pt/\gamma–Al_2O_3$ catalysts. Electrochemically prepared materials demonstrated catalytic activity comparable to that of conventional impregnated catalyst and reasonable stability.

Graphical Abstract

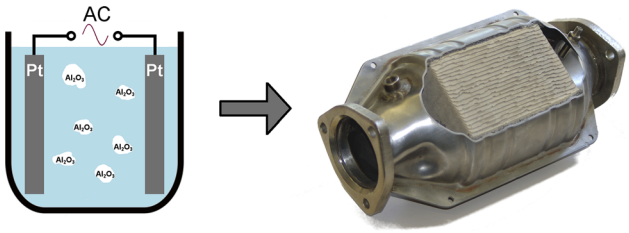

Keywords Platinum · DOC · Electrochemical dispersion · Oxidation

1 Introduction

Application of diesel engines in road vehicles has several advantages, the most important of which are high fuel efficiency and significantly reduced carbon monoxide emissions compared to gasoline engines. However, apart from CO and hydrocarbons, diesel engines produce noticeable amounts of particulate matter (soot) and nitrogen oxides (mainly NO) which present a hazard to the environment and should be abated [1]. These pollutants are removed by a combination of catalysts installed in the exhaust system among which the so-called diesel oxidation catalyst (DOC) is responsible for the oxidation of CO, hydrocarbons and NO to CO_2, water and NO_2 [2]. NO_2 is used downstream to facilitate oxidation of soot over the diesel particulate filter (DPF) [3] and can also be used to promote removal of NO by the selective catalytic reduction (SCR) [4].

The CO oxidation activity of Pt catalysts is a structure sensitive reaction and, therefore strongly depends on the Pt

Electronic supplementary material The online version of this article (doi:10.1007/s10562-015-1651-z) contains supplementary material, which is available to authorized users.

✉ Dmitry E. Doronkin
dmitry.doronkin@kit.edu

1 Institute of Catalysis Research and Technology, Karlsruhe Institute of Technology, Hermann-von-Helmholtz-Platz 1, 76344 Eggenstein-Leopoldshafen, Germany

2 Institute for Chemical Technology and Polymer Chemistry, Karlsruhe Institute of Technology, Engesserstr. 20, 76131 Karlsruhe, Germany

3 Platov South-Russian State Polytechnical University, 132 Prosveschenia St., Novocherkassk, Russia 346428

4 Physics Department, Southern Federal University, 5 Zorge St., Rostov-on-Don, Russia 344090

5 National University of Science and Technology MISiS, Leninskiy pr. 4, Moscow, Russia 119049

particle size [5, 6]. Hence, CO adsorbed on the step and terrace Pt sites shows varying reactivity [7] which also results in different activities of Pt particles of different shapes. Furthermore, the turnover frequency (TOF) of CO oxidation increases with increasing particle size up to a certain limit. As the fraction of accessible surface Pt atoms decreases for larger particles the rate of CO oxidation normalized per total amount of Pt (TOF) also decreases. The decrease in surface Pt atoms is responsible for catalyst deactivation as a result of thermal aging [8].

NO oxidation also depends on the Pt particle size and is, therefore, also structure sensitive. Catalysts with bigger Pt particles (i.e. after catalyst aging) show higher specific NO oxidation activity [5]. Furthermore, the oxidation state of Pt was shown to correlate with NO oxidation activity [9]. In the exhaust, CO and NO are both present and compete for the active Pt sites which highlights the need for testing catalysts during simultaneous oxidation of CO and NO. In general, trends known for individual CO and NO oxidation processes are preserved but the conversion profiles shift along the temperature axis. The presence of CO was shown to increase NO oxidation activity at lower temperatures [10], while at the same time CO oxidation activity decreased [5].

The size and shape of Pt particles and, thus, the catalytic activity are defined by the synthesis method [11–13], pretreatment conditions [14], aging [5] and even the actual gas environment [15, 16]. Aging of automotive Pt-containing catalysts leads mainly to sintering, i.e. growth of Pt particles [5, 8, 9, 17]. Pt sites on bigger particles are more active with respect to oxidation reactions but the relative amount of surface Pt decreases with increasing particle size (as a result of sintering) leading to the catalyst deactivation. The rate of sintering of Pt nanoparticles was shown to depend on the uniformity of particle size distribution. Catalysts with narrow uniform particle size distribution were deactivated slower compared to those with wide particle size distribution [18]. This emphasizes the need for catalyst synthesis techniques which are inexpensive, reproducible and offer particle size and shape control with narrow uniform particle size distribution.

Several techniques for synthesis of Pt catalysts exist. The most common is the incipient wetness impregnation for which a metal precursor is dissolved and a precise amount of the solution is then brought into the pores of the support material. A variety of platinum precursors are used for this purpose with the most common being H_2PtCl_6 [12, 19–21], $Pt(acac)_2$ [12], and $Pt(NH_3)_4(NO_3)_2$ [19, 22]. Impregnation with H_2PtCl_6 may alter the acidity of the support and lead to poisoning by chlorine residues [23, 24], usage of acetylacetonate leads to high dispersion of platinum but also alters acidity of the support [12]. Furthermore, H_2PtCl_6 precursor is highly hygroscopic and cannot be stored for long periods of time. This can be overcome by preparing first stable colloidal solution of Pt nanoparticles with their subsequent deposition [25]. Although the colloidal technique allows tuning particle size of Pt, it is not simple and easy to scale up. The other possibility of tuning nanoparticle size is altering catalyst calcination and reduction conditions [22]. Flame spray pyrolysis (FSP) is another technique able to produce supported Pt catalysts with high dispersion and high activity [26, 27] which, on the other hand, leads to a formation of oxidized Pt species and requires a reduction step. FSP also involves burning significant amount of organic solvents which makes it not compatible with "green chemistry" principles. Platinum-containing supported catalysts may also be synthesized using a single-step sol–gel technique [28, 29] which results in active catalysts but may lead to encapsulation of some Pt in the support.

Recently an electrochemical dispersion procedure (not to be confused with electroless [30] or electrochemical [31] deposition where platinum is deposited from a solution of a precursor salt) was used to produce Pt/C electrocatalyst [32]. This one-step technique is remarkably simple and does not require additional calcination and reduction of the final catalyst. Furthermore, Pt foil is used as a Pt precursor which reduces costs and ensures absence of contaminants able to change catalyst performance (e.g. Cl in [24]). In this paper we have studied the applicability of the electrochemical dispersion technique for the production of Pt/Al_2O_3 oxidation catalysts with low Pt loading. The catalysts were thoroughly characterized by X-ray diffraction (XRD), X-ray absorption near edge structure (XANES) and extended X-ray absorption fine structure (EXAFS) spectroscopy, transmission electron microscopy (TEM), and CO chemisorption. The materials were also tested with respect to CO and NO oxidation in the fresh state as well as after aging in order to assess their activity and stability.

2 Experimental Part

2.1 Catalyst Synthesis

Electrochemical method (EL catalysts): For preparation of Pt/Al_2O_3 catalysts a method based on metal dispersion under pulse alternating current (AC) conditions in alkaline solution was used. This "one pot" electrochemical method has been successfully utilized for the synthesis of electrochemical catalysts in previous works in which highly efficient Pt/C [32] and Pt_3Ni/C [33] catalysts for low temperature fuel cells were successfully prepared. The electrochemical cell (100 ml beaker) has two Pt foil electrodes (0.25 mm thickness, approx. 0.6 g each) immersed in a suspension of 1 g of γ-Al_2O_3 powder (SASOL SCFa-

230, $S_{BET} \sim 230$ m^2/g) in 50 ml 2 M NaOH aqueous solution. The electrodes are connected to a pulse AC source operating at 50 Hz and average current density 1 A/cm^2. The suspension was stirred with a magnetic stirrer (approx. 350 rpm) during the synthesis. Pt loading in the catalyst was controlled by the duration of the synthesis process (2–7 min) which resulted in loadings of 0.81 and 3.8 wt% Pt (EL-1 and EL-4 catalysts, respectively). Finally, the catalysts were rinsed with H_2O to a neutral pH and dried at 80 °C for 1 h.

Incipient wetness impregnation method (IWI catalyst): For a comparison 2 wt% Pt/Al_2O_3 prepared by traditional incipient wetness impregnation was used. γ-Al_2O_3 from the same batch as in case of electrochemically-synthesized catalysts was used as a support. The support was impregnated with hexachloroplatinic acid ($H_2PtCl_6 \cdot xH_2O$), the catalyst was then dried overnight at 70 °C and calcined for 2 h at 500 °C. Finally, the catalyst was reduced in 5 % H_2/He (2 h at 400 °C) analogously to [34].

2.2 Catalyst Testing

Catalytic tests were carried out in a fixed-bed quartz flow reactor (inner diameter 8 mm) in a temperature programmed mode while the temperature was cycled between 50 and 250 °C (for CO oxidation) and between 50 and 500 °C (for NO and CO/NO oxidation) at 5 °C/min. The temperature was controlled using an Eurotherm 2416 temperature controller with a K-type thermocouple. 30 mg of catalyst (sieve fraction 100–200 μm) was diluted with 700 mg of quartz and placed on a quartz wool bed. The bed height was ~12 mm and the gas flow 500 ml/min (GHSV: 690,000 h^{-1} for the catalyst only and 12,500 h^{-1} for the whole catalyst bed with quartz). The gas composition contained 1000 ppm CO and/or 1000 ppm NO, and 10 % O_2 in nitrogen. Reaction products were analyzed by an MKS 2030 FTIR analyzer. Prior to the testing and before changing the feed composition catalysts were pretreated in 5 % H_2 in N_2 flow at 160 °C for 10 min to clean the Pt surface from possible adsorbates. This rather low pretreatment temperature for catalytic and X-ray absorption studies was chosen in order to minimize potential changes in Pt nanoparticles size. Heating and cooling cycles during CO oxidation were performed twice. The results of both test cycles were similar, and in order to ensure the same starting state of the catalyst surface, the results from the second cycle are reported in the paper.

CO conversion was calculated using the following equations:

$$X_{CO} = 1 - \frac{C_{CO}^{outlet}}{C_{CO}^{inlet}} = \frac{C_{CO_2}^{outlet}}{C_{CO}^{inlet}} \quad (1)$$

where C_{CO}^{inlet}, C_{CO}^{outlet} and C_{CO2}^{outlet} denote CO and CO_2 concentrations at the inlet and outlet of the reactor, where:

$$C_{CO}^{inlet} = C_{CO}^{outlet} + C_{CO_2}^{outlet}. \quad (2)$$

NO conversion to NO_2 was calculated in the same way as CO conversion.

For the assessment of the catalyst stability a mild aging technique previously described by Boubnov et al. [5] was chosen. According to this procedure, the catalyst was exposed to a 10 % O_2, 5 % H_2O, N_2 (rest) mixture at 600 °C for 1 h, cooled down and further pretreated in 5 % H_2 in N_2. Afterwards, the catalytic tests were repeated.

2.3 CO Chemisorption

Pt dispersion was evaluated using a technique proposed by Karakaya and Deutschmann [35]. The same setup as for the catalyst testing was used for CO chemisorption experiments. After pretreatment of the catalyst in 5 % H_2 in N_2 flow at 160 °C for 10 min the reactor was cooled down to 40 °C and CO was adsorbed. The reactor was then flushed with N_2 for 30 min (total flow 300 ml/min), and a TPD (temperature-programmed desorption) up to 500 °C was started with a temperature ramp of 15 °C/min. Pt dispersion was calculated based on the amount of desorbed CO and CO_2 (integrated between 50 and 250 °C) and the metal/CO adsorption stoichiometry 1:1.

The surface-averaged Pt nanoparticle sizes (d_S, nm) were calculated from the dispersion (D) assuming a hemispherical shape and using atomic parameters for Pt as suggested by Spenadel and Boudart [36]. This results in the final relation (3).

$$d_s = \frac{1.02}{D}. \quad (3)$$

2.4 X-ray Absorption Spectroscopy (XAS)

X-ray absorption spectra (XANES and EXAFS) were recorded at the XAS beamline at the ANKA synchrotron radiation source in transmission (before catalytic tests) and fluorescence (after aging and catalysis) modes. The catalysts (pressed and sieved to 100–200 μm grains) were placed in in situ microreactors (quartz capillary, 1.5–3 mm diameter, 20 μm wall thickness) heated by a hot air blower (Gas Blower GSB-1300, FMB Oxford) [37]. The beam size was kept at 6 × 1 mm. Before the measurements the catalysts were pretreated for 15 min at 150 °C in a flow of 75 ml/min 5 % H_2 in He, after which they were cooled down to 25 °C in a flow of 5 % H_2 in He, and EXAFS spectra at Pt L_3 edge (11,564 eV) were recorded. The

measurement of IWI catalyst after CO oxidation cycle was done in a flow of 50 ml/min of 1000 ppm CO, 10 % O_2 in He after performing heating to 200 °C and cooling to room temperature. The spectra were normalized and the extended X-ray absorption fine structure spectra (EXAFS) background subtracted using the ATHENA program from the IFFEFIT software package [38]. The average Pt oxidation state was determined by a linear combination analysis of the X-ray absorption near edge structure (XANES) spectra using Pt foil and PtO_2 as reference spectra in a fitting range of 11,544–11,594 eV.

The k^1-, k^2-, and k^3-weighted EXAFS functions were Fourier transformed in the k range of 3.0–13 $Å^{-1}$ and multiplied by a Hanning window with sills size of 1 $Å^{-1}$. The structural model was based on a Pt metal core (ICSD collection code 64923) and an oxide shell modeled using PtO_2 (ICSD collection code 4415). The structure refinement was performed using ARTEMIS software (IFFEFIT) [38]. For this purpose the corresponding theoretical backscattering amplitudes and phases were calculated by FEFF 6.0 [39]. The theoretical data were then adjusted to the experimental spectra by a least square method in R-space between 1.4 and 3 Å (corresponding to the first Pt–O and Pt–Pt shells). First, the amplitude reduction factors ($S_0^2 = 0.8$ (O) and 0.82 (Pt)) were calculated using spectra of Pt foil and PtO_2 model compounds and then the coordination numbers, interatomic distances, energy shift (δE_0) and mean square deviation of interatomic distances (σ^2) were refined. The absolute misfit between theory and experiment was expressed by ρ.

2.5 X-ray Diffraction (XRD)

X-ray diffractograms of catalyst powders were acquired using a Bruker D8 Advance diffractometer with Cu Kα radiation, a rotating sample holder, step size 0.016°, and 2 s/step integration time. The resulting patterns were smoothed using the Savitzky–Golay filter using 2nd order polynom and a 9-point window.

2.6 Transmission Electron Microscopy (TEM)

Powder samples of the catalysts were ultrasonically dispersed in ethanol or isopropanol and one drop of the suspension was dried on a copper grid covered with holey carbon film. The aged EL-4 catalyst was thoroughly ground in a mortar and supported on a TEM grid in dry form (because of admixtures of quartz grains used during catalyst testing). The catalyst specimens were examined in a FEI Titan 80-300 aberration corrected electron microscope operated at 300 kV. The particle size was defined as a major axis of an ellipse containing the particle.

2.7 Atomic Absorption Spectroscopy (AAS)

Pt content in the synthesized catalysts was determined by atomic absorption spectroscopy using a Hitachi-Zeeman Z-2000 spectrometer. For the measurements catalysts were dissolved in a mixture of nitric and hydrochloric acids (1:3 volume ratio) and then diluted with deionized water.

3 Results

3.1 Catalyst Characterization

The results of AAS and CO chemisorption are summarized in Table 1 along with surface averaged particle sizes calculated from Pt dispersion. The particle size values derived from chemisorption should be interpreted with caution as they assume uniform distribution of spherical particles which is not the real case as one can see from TEM ([40], see also TEM results below), therefore these particle sizes are useful rather to indicate trends. The slightly higher than expected Pt concentration in the IWI catalyst can be a result of dehydration of the parent alumina during the calcination step.

XANES and EXAFS spectra of the fresh IWI and EL catalysts, pretreated in H_2 in the same way as it was done for the catalytic tests, are shown in Fig. 1. The pretreatment was aimed at cleaning the surface of Pt nanoparticles from adsorbed species, most importantly, CO_2 and oxygen. Table 2 summarizes the results of XANES and EXAFS analysis. For fitting the EXAFS spectrum of the IWI catalyst a model with an oxygen shell analogous to PtO_2 [41] and one Pt shell as in the metallic Pt was used. The average coordination number of the Pt–Pt shell in the IWI catalyst is very low (6) indicating small particle size or a small fraction of metallic nanoparticles among the disordered PtO_x clusters. A shorter Pt–Pt bond also indicates very small clusters in this case. The data is in line with the high dispersion of Pt in the fresh IWI catalyst as determined by CO chemisorption.

The spectra of EL catalysts can also be modeled using one oxygen and one platinum shells. In case of the EL-1 catalyst the Pt–Pt coordination number is ca. 6 which is similar to the IWI case, but taking into account higher number of oxygen atoms and relatively high average Pt oxidation state we assume a model of Pt metallic core (Pt–Pt bond distance corresponds to metallic particles) and an oxide (or chemisorbed oxygen) shell.

Increasing synthesis duration resulted in the EL-4 catalyst with higher Pt loading. Along with an almost fivefold increase in Pt loading, the average Pt–Pt coordination size increased to approx. 9.5. On the other hand, the average oxidation state of Pt in the catalyst decreased significantly,

Table 1 Summary of the catalyst characterization by AAS, CO-chemisorption and the resulting estimated particle size

Catalyst	Resulting Pt loading by AAS (wt%)	Pt dispersion (D) as determined by CO chemisorption		Surface averaged particle size (d_S, nm) estimated from Pt dispersion	
		Fresh catalyst	Aged catalyst	Fresh catalyst	Aged catalyst
IWI	2.19	0.85	0.25	1.2	4.1
EL-1	0.81	0.63	0.53	1.6	1.9
EL-4	3.8	0.22	0.11	4.6	9.0

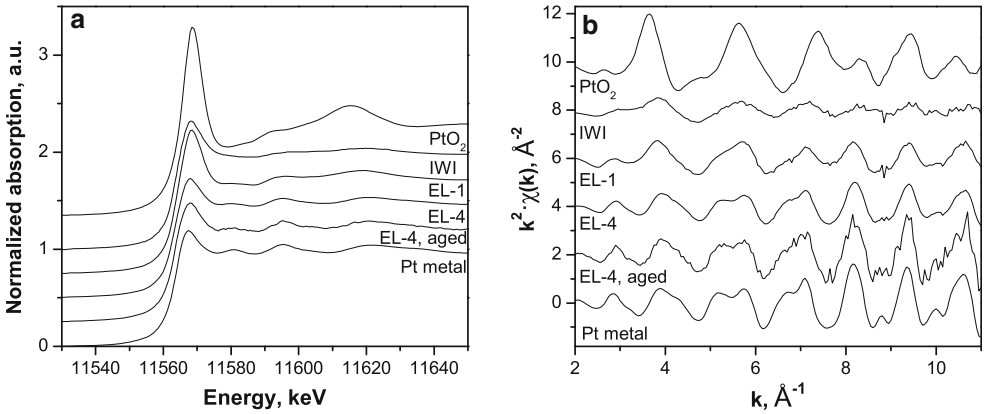

Fig. 1 **a** XANES and **b** k^2-weighed EXAFS spectra for all studied fresh catalysts as well as EL-4 sample after catalysis and aging, including spectra of reference compounds (Pt metal and PtO_2)

Table 2 Average Pt oxidation states and coordination environments determined from XANES and EXAFS spectra

Catalyst	Pt oxidation state*	Pt-O distance (Å)	Coordination number (O)	Pt–Pt distance (Å)	Coordination number (Pt)	σ^2 (10^{-3} Å^2)	δE_0 (eV)	ρ (%)
IWI	+0.66 ± 0.10	1.99 ± 0.04	1.2 ± 0.5	2.71 ± 0.02	6.0 ± 2.1	11 ± 3	6.6 ± 3.2	4.3
EL-1	+1.44 ± 0.05	2.01 ± 0.03	1.8 ± 0.5	2.78 ± 0.01	5.9 ± 1.9	5 ± 2	12.0 ± 2.6	3.0
EL-4	+0.26 ± 0.02	1.94 ± 0.035	0.4 ± 0.2	2.76 ± 0.004	9.4 ± 0.7	6 ± 0.5	8.7 ± 0.7	0.2
EL-4 aged	+0.26 ± 0.02	–	–	2.77 ± 0.004	11.5 ± 1.1	4 ± 0.5	9.0 ± 0.8	0.3

* Determined by linear combination analysis of XANES spectra after pretreatment with 5 % H_2/He at 150 °C

rendering the particles almost purely metallic. After aging the low oxidation state of Pt was preserved and Pt particles sintered, resulting in an average Pt–Pt coordination number around 11.5.

The X-ray diffractograms of the studied catalysts are shown in Fig. 2a and the Pt (111) signals after subtraction the diffraction pattern of the parent alumina are shown in Fig. 2b. It is hardly possible to detect crystalline Pt in the IWI catalyst since only reflections of γ-Al_2O_3 are observable [42]. The absence of Pt reflections in the IWI catalyst agrees well with the very small oxidized Pt clusters as observed by XAS and TEM (see below). Small contributions from the Pt (111) reflection can be seen in the diffractogram of EL-1 after subtracting the pattern of parent alumina (Fig. 2b). The diffractogram of the EL-4 catalyst, on the contrary, reveals Pt (111) and (311) reflections at approx. 39.8° and 81.5° correspondently [43]. Additionally, the intensity of a signal at approx. 46.5° increases relative to those found in the diffractograms of IWI and EL-1 due to the superimposed reflections from γ-Al_2O_3 (400) and Pt (200). For catalysts with low metal loadings quantitative evaluation of XRD results may be not reliable due to a large fraction of particles smaller than 2 nm which are not detected by XRD and also because of overlapping Pt and γ-Al_2O_3 reflections in our case. Therefore, especially for IWI and EL-1 catalysts, particle sizes and

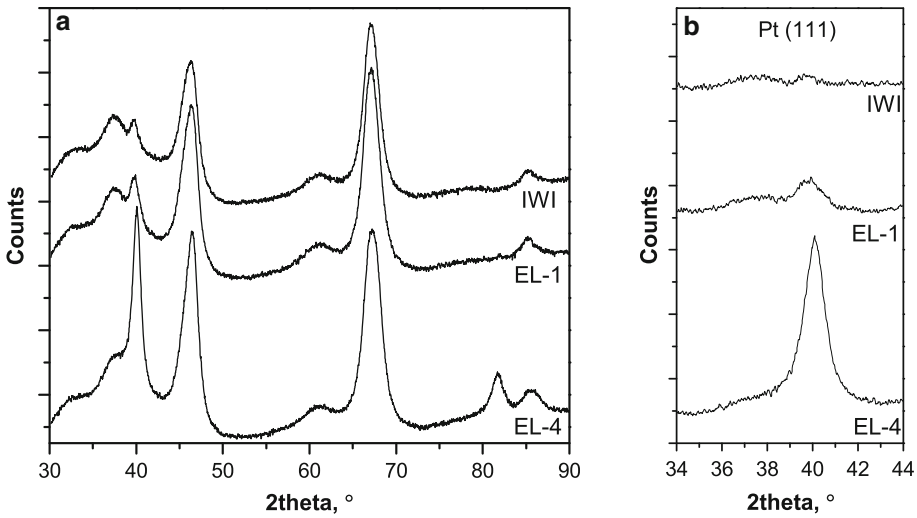

Fig. 2 **a** X-ray diffractograms of the studied catalysts (fresh state). **b** Reflection from the Pt (111) crystal plane after subtraction of the diffractogram of the parent alumina

dispersion obtained from TEM (see below) and CO chemisorption are used.

TEM images of the studied catalysts and the derived particle size distributions are shown in Fig. 3. The IWI catalyst contains very small (ca. 0.6–1.0 nm) particles with rather narrow size distribution (Fig. 3a). The electrochemically made catalyst with the lowest Pt loading, EL-1, has Pt nanoparticles of about 3 nm size with a broader size distribution (Fig. 3b). The total number of Pt particles visible in the TEM images of EL-1 sample is small and they are unevenly distributed on the support. Fresh EL-4 shows mostly particles of about 4 nm but also bigger agglomerates up to 50 nm with a broad size distribution. Another feature of the EL-4 catalyst is the uneven distribution of Pt nanoparticles on the alumina support, with some regions of the support almost free of particles (clearly visible on Fig. 3c) underlining that γ-Al_2O_3 is a much more demanding support than carbon [32]. It should be noted that average Pt nanoparticle sizes in the EL catalysts did not show any significant dependence on the Pt loading unlike catalysts prepared by the commonly used impregnation technique [44, 45]. Aging of the EL-4 catalyst led to a very broad bimodal size distribution (Fig. 3d) with many rather small particles ($\sim$2 nm), around 25–30 % of particles around 6 nm, and occasionally large agglomerates (up to 30 nm).

3.2 Catalysis

Synthesized catalysts were further tested with respect to oxidation of CO, NO and simultaneous oxidation of CO and NO, which models diesel exhaust conditions. The conversion profiles for CO (both in the absence and presence of NO) and NO (in the absence of CO) are shown in Fig. 4 for fresh (left) and aged (right) catalysts. NO conversion profiles in the presence of CO are not reported as the trends are the same as obtained without CO.

The CO conversion profiles show the typical behavior of Pt/Al_2O_3 catalysts with a steep light-off profile and a hysteresis between heating and cooling steps. The fresh IWI catalyst shows rather low CO oxidation activity (Fig. 4a), comparable to the EL-1 catalyst with much lower Pt loading. Moreover, the fresh IWI catalyst is different from all others showing an "inverse" hysteresis with lower CO oxidation activity during cooling than during heating. In addition to this, oscillations of CO conversion were observed during cooling. Such behavior has been previously reported for Pt/Al_2O_3 catalysts prepared by incipient-wetness impregnation [34] and attributed to very small Pt particles with low CO oxidation activity. Although the XANES data indicated a high degree of Pt reduction (Table 2) in the pretreated IWI catalyst before catalytic testing, small Pt particles in this catalyst are easily oxidized during catalysis which may be the reason for the observed low activity and the "inverse" hysteresis of CO oxidation. For instance, oxidation state of Pt in the IWI catalyst was measured by the in situ XAS immediately after one CO oxidation cycle (heating and cooling) and shown to be $+1.18 \pm 0.12$ which is higher than $+0.66 \pm 0.10$ in the H_2-pretreated sample.

Mild aging leads to sintering of Pt particles with an increase in average particle size (Table 1) and decrease in Pt dispersion. This results in an overall decrease in catalytic activity but the shift of EL light-off curves toward higher temperatures is more pronounced than for the IWI catalyst (Fig. 4b). The decrease in catalytic activity in case of the EL catalysts is solely due to sintering of Pt as demonstrated by CO chemisorption, TEM and EXAFS. On the other hand, sintering of Pt particles in the IWI catalyst tentatively leads to formation of Pt nanoparticles less prone

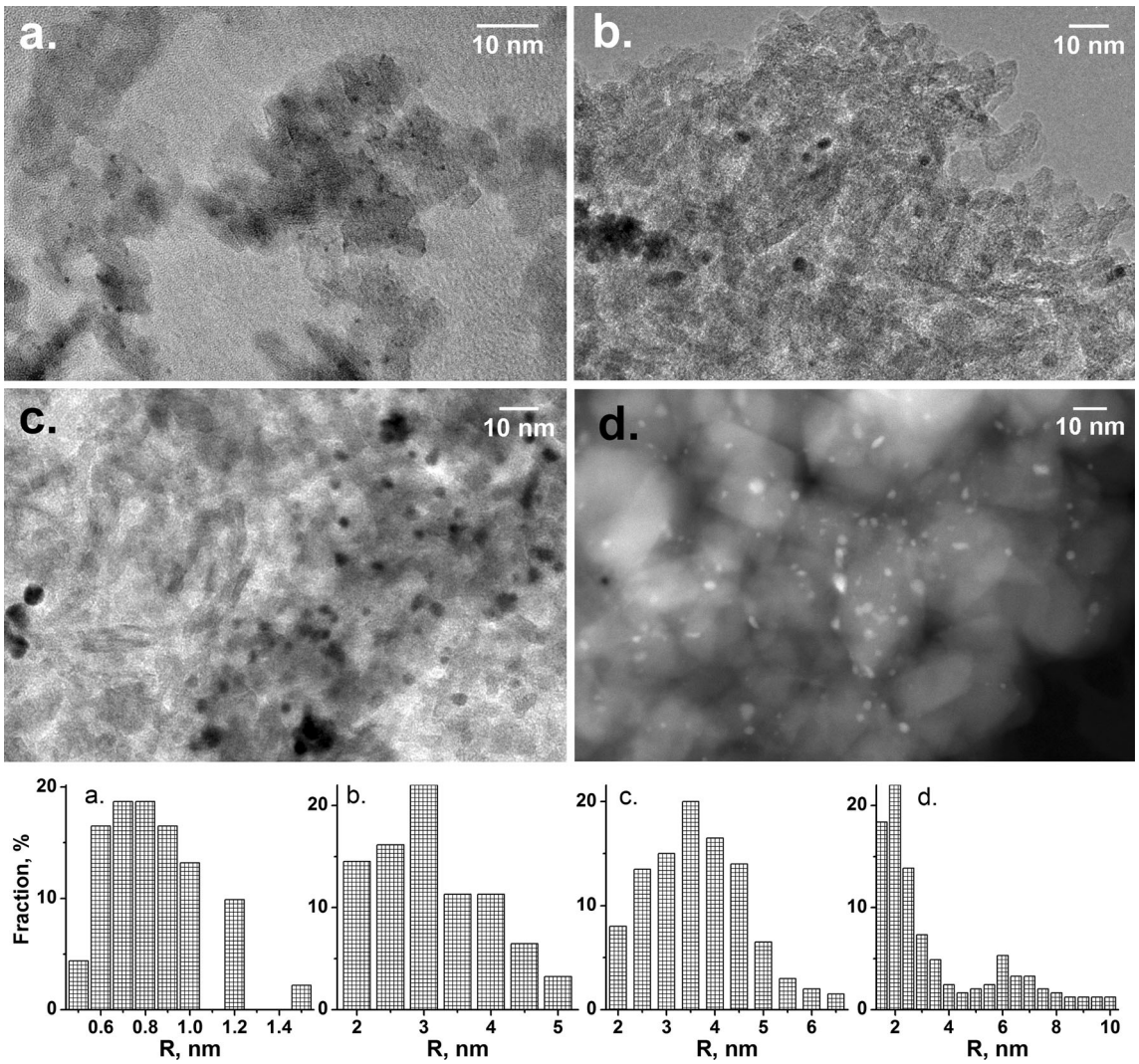

Fig. 3 **a**–**c** TEM and **d** STEM–HAADF images (*top*) and particle size distribution (*bottom*) for fresh: **a** IWI, **b** EL-1, **c** EL-4, and **d** aged EL-4 catalysts. Number of particles analyzed to obtain particle size distribution was 93 for IWI, 62 for EL-1, 200 for EL-4, and 245 for aged EL-4 catalysts

to oxidation under reaction conditions and therefore more active. Thus, the combination of two factors—a lower total amount of surface Pt sites and higher resistance of Pt particles to oxidation—keeps the activity of the IWI catalyst just slightly changed. Since diesel oxidation catalysts may be exposed to temperatures as high as 800 °C we performed an additional test after aging in humid air at 800 °C for 1 h. Such severe aging did result in a further deactivation of all catalysts but did not change the relative activity trend (test conditions and results are available in the Electronic Supporting Information, Fig. S1, note the different GHSV).

Similar trends are reported for NO oxidation over fresh and aged catalysts (Fig. 4c, d). In this case, the fresh IWI catalyst shows very low activity due to small Pt particles and gains much higher activity after aging in line with the increase in Pt particle size observed by CO chemisorption (Table 1) and the reported structure sensitivity of NO oxidation [5]. EL catalysts appear to keep rather stable NO oxidation activity in spite of aging which may be due to the big particle size already in the fresh catalysts. Furthermore, according to the TEM (Fig. 3b) Pt particles in EL-1 are well separated from each other on the alumina support which prevents strong sintering (Table 1).

CO oxidation in the presence of NO (CO + NO oxidation) occurs at higher temperatures similar to the temperatures of NO oxidation. Moreover, during CO and NO oxidation activity differences between both fresh and aged catalyst series level off (Fig. 4e, f). In this case IWI catalyst with the highest Pt dispersion and smallest particles shows CO (and NO) light-off in the same temperature range as EL-4 and the light-off of EL-1 is shifted toward

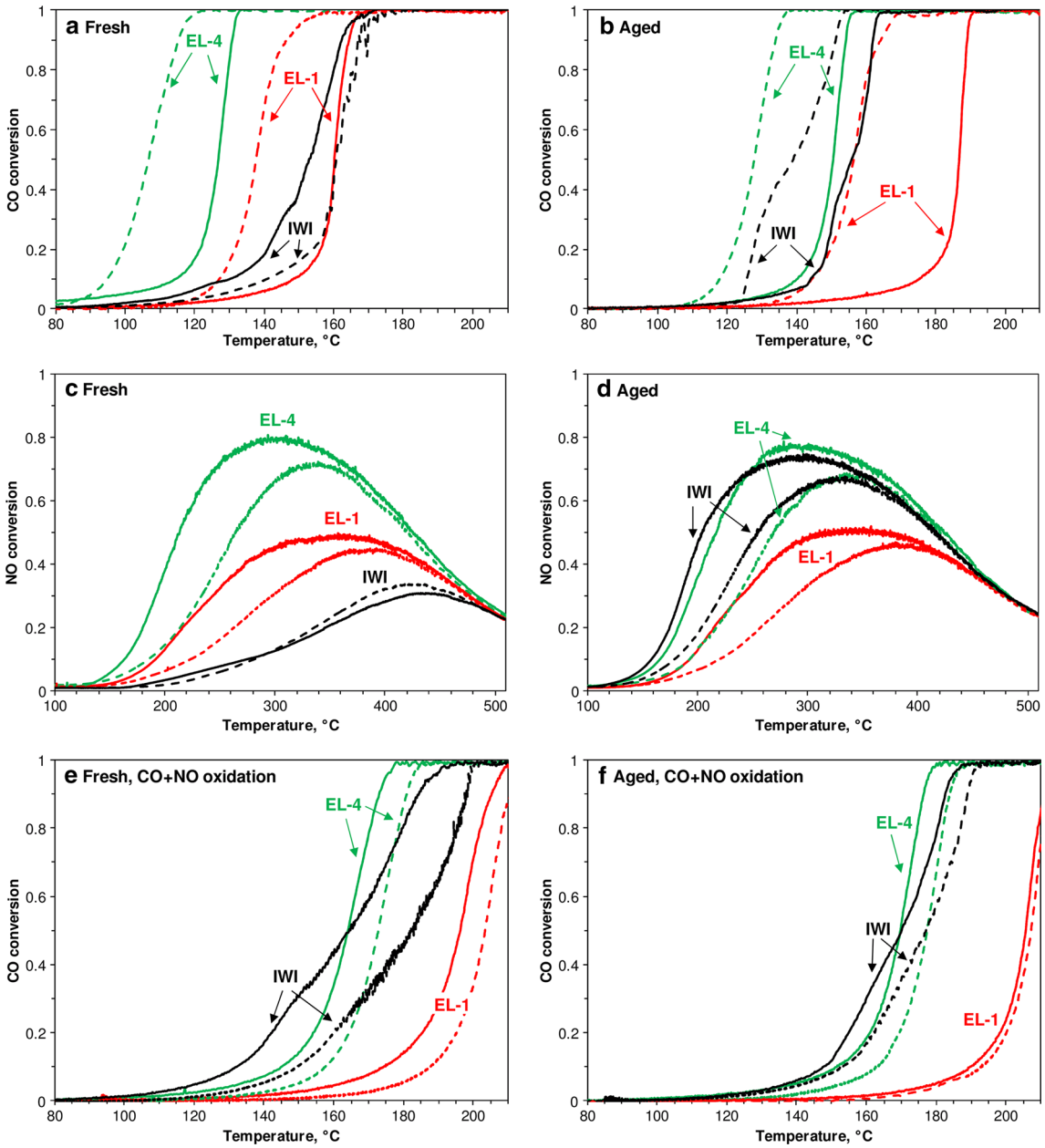

Fig. 4 **a**, **b** Conversion of CO obtained during CO oxidation; **c**, **d** conversion of NO obtained during NO oxidation; **e**, **f** conversion of CO obtained during CO and NO simultaneous oxidation. *Solid lines* are recorded during heating, *dashed lines* during cooling. Conditions: 1000 ppm CO or (and) 1000 ppm NO, 10 % O_2 in N_2, 30 mg of catalyst, 500 ml/min flow

high temperatures due to rather low Pt loading in this sample.

4 Discussion

The aim of this study is to thoroughly characterize new catalysts and test their catalytic activity in oxidation of CO and NO in order to prove the ability of the electrochemical dispersion technique to produce active Pt/Al_2O_3 oxidation catalysts. To achieve this goal several catalyst samples were synthesized, thoroughly characterized to be able to explain the observed activity differences and tested in catalysis. Electrochemical dispersion technique proved to be reproducible and EXAFS spectra of several catalysts with Pt loadings in the range 3–10 wt% (see Electronic Supporting Information) proved to be almost identical which points out the same size and structure of Pt nanoparticles independently on Pt loading (unlike catalysts made by incipient wetness impregnation [44, 45]). The

only property depending on the Pt loading appeared to be the average Pt oxidation state (Table 2) which decreases with increasing Pt loading. XAS measurements on a series of samples (Fig. S2 in ESI) suggested the formation of a small portion of oxidized PtO_x (corresponding to 0.25 ± 0.03 wt% Pt in form of PtO_2) in all samples if other synthesis conditions are kept unchanged and lower amount of oxidized Pt when higher amount of alumina was used for synthesis. Hence, while the amount of oxidized Pt stays unchanged and the overall Pt loading increases, average Pt oxidation state decreases. And this small portion of oxidized Pt is believed to originate from the surface of Pt electrodes which is corroded and dispersed in the first seconds of the synthesis. This allows predicting lower average Pt oxidation state if higher amount of alumina support is introduced during the synthesis as needed for scaling up the synthesis. This was indeed confirmed during the synthesis using 2 g of Al_2O_3 instead of 1 g which resulted in 0.17 wt% Pt in form of PtO_2.

Since CO and NO conversion profiles over Pt/Al_2O_3 catalysts are determined by a combination of parameters, i.e. amount of surface platinum atoms, their intrinsic activity (TOF) etc., the given conversion profiles cannot be used directly to judge the catalyst performance. The matter becomes even more complicated as platinum loading in the catalysts also differs. Hence, the amount of surface Pt atoms available for reactants was determined by CO chemisorption and used to calculate the specific activity of surface Pt sites (TOF) defined as the number of CO (or NO) molecules converted per surface Pt site per second. However, for the given dataset there is no single temperature point at which TOF can be calculated for all three catalysts (due to different light-off temperatures). Therefore, TOFs obtained during heating were linearized using Arrhenius plots (assuming power law kinetics of CO and NO oxidation [46, 47]) in the region of low conversions (CO conversion: 1–5 %; NO conversion: 2–4.5 %) so that the concentration gradients can be neglected (Fig. 5). Apparent activation energies determined from Arrhenius plots are reported in Table 3.

In the ideal case, if CO oxidation activity depends only on the number of active sites which all have the same activity (i.e. no structure sensitivity), the plots in Fig. 5a should fit to a single trend line. Most of the catalysts fit reasonably well to a single trend except aged EL-1 and fresh EL-4 samples. Apparent activation energies for CO oxidation lie in the range 70–90 kJ/mol. The plot of aged EL-1 activity is shifted to lower values but demonstrates similar activation energy (Table 3) which may originate from an error in estimation of number of Pt sites (since the absolute number of Pt sites in this sample is very small). The activation energy for the fresh EL-4 catalyst is significantly lower than for other samples which may indicate significant mass-transfer limitations due to a very active catalyst. The single trend for all catalysts means that the catalyst activity with respect to CO oxidation scales with the amount of surface Pt sites, i.e. the specific activity of those sites is similar, independent of the catalyst synthesis technique and the pretreatment (in this case aging). The only way aging influences the CO oxidation activity in this case is by decreasing the amount of surface Pt. The structure sensitivity is not observed here.

Similar activation energies are obtained for NO oxidation over the IWI and EL-1 catalysts (Table 3) but in this case they differ for fresh and aged catalysts. The difference is even stronger for the EL-4 catalyst. The difference in E_a (Fig. 5b) proves that NO oxidation is indeed structure sensitive, analogous to [48]. The extremely low activity of the fresh IWI catalyst (Fig. 5b) is attributed to the very small size of Pt clusters making them rather inactive for NO oxidation (according to the structure sensitivity). This may be due to oxygen chemisorption on the low coordinated Pt sites resulting in less active sites for NO oxidation [47, 49]. Low activity of fresh IWI may also be related to traces of Cl due to the use of Cl-containing precursor for catalyst synthesis [50, 51].

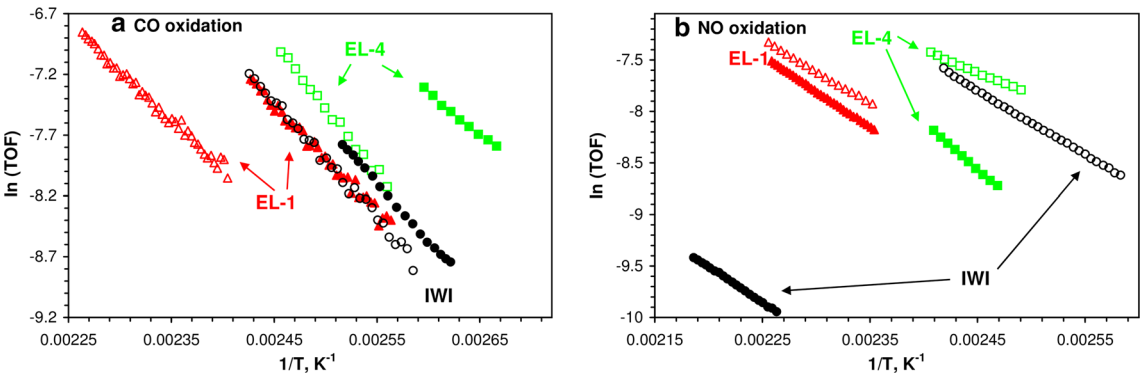

Fig. 5 Arrhenius plots of **a** CO and **b** NO oxidation rate normalized per amount of active sites (TOF) obtained from CO chemisorption. *Filled symbols* represent fresh catalysts, *empty symbols*—catalysts after aging

Table 3 Apparent activation energies for CO and NO oxidation (estimated using conversion data obtained during heating)

Catalyst	E_a (CO oxidation), kJ/mol (±3 kJ/mol)		E_a (NO oxidation), kJ/mol (±3 kJ/mol)	
	Fresh catalyst	Aged catalyst	Fresh catalyst	Aged catalyst
IWI	79	80	58	52
EL-1	72	68	58	51
EL-4	56	89	75	36

The fact that intrinsic activity of Pt sites in catalysts prepared using the electrochemical dispersion approach is similar to that of the conventionally-prepared catalyst makes them suitable for application as oxidation catalysts. Hence, taking into account the following advantages of the electrochemical dispersion technique one can successfully use it for the synthesis of supported metallic heterogeneous catalysts. First of all, using Pt foil guarantees absence of contaminating species which may compromise the activity of the resulting catalyst. Second, the technique does not require calcination and reduction steps which saves energy and costs for gases and gas dosing infrastructure. Electrochemical dispersion results in intermediately-sized nanoparticles even for supports which favor very high dispersion of the metal like the one used in this study [52]. Due to structure sensitivity, a certain minimum size of Pt nanoparticles is required for the catalyst to be active in CO and NO oxidation which makes electrochemically-synthesized catalysts suitable for application as diesel oxidation catalysts (DOC). On the other hand, for the large-scale industrial application, the Pt distribution should be improved and the possibility to control of size of Pt nanoparticles has yet to be explored.

5 Conclusions

The possibility of application of electrochemical dispersion technique for the production of Pt/Al_2O_3 oxidation catalysts was evaluated. The method is fast, simple and does not require calcination and reduction steps. Characterization by XAS, XRD, TEM, and CO chemisorption showed that electrochemical dispersion results in producing relatively large 3–4 nm (average) Pt nanoparticles on a high surface area γ-alumina, which are active in both CO and NO oxidation. In contrast to the conventional catalyst made by incipient-wetness impregnation, larger Pt nanoparticles prepared by electrochemical dispersion show higher activity in the structure-sensitive NO oxidation. Hence, in future this preparation method should be applied to other metals and supports.

Acknowledgments The authors thank ANKA synchrotron radiation source (KIT, Karlsruhe) for providing beamtime at the XAS beamline and Dr. Stefan Mangold for help during measurements. Angela Beilmann (KIT) is acknowledged for the AAS measurements, and Gülperi Cavusoglu for XRD data acquisition. The authors would further like to thank the Federal Ministry of Education and Research (BMBF) for the financial support (Project "Materials in Action"), and Dr. A. Malyschew (SASOL) for fruitful discussions. Nina V. Smirnova and Alexandra B. Kuriganova thank the Russian Science Foundation (Project No. 14-23-00078) for the financial support.

References

1. Acres GJK (1970) Platinum catalysts for diesel engine exhaust purification. Platin Met Rev 14:78–85
2. Johnson TV (2009) Review of diesel emissions and control. Int J Engine Res 10:275–285. doi:10.1243/14680874jer04009
3. Bueno-López A (2014) Diesel soot combustion ceria catalysts. Appl Catal B Environ 146:1–11. doi:10.1016/j.apcatb.2013.02.033
4. Nova I, Ciardelli C, Tronconi E et al (2006) NH_3–NO/NO_2 chemistry over V-based catalysts and its role in the mechanism of the fast SCR reaction. Catal Today 114:3–12. doi:10.1016/j.cattod.2006.02.012
5. Boubnov A, Dahl S, Johnson E et al (2012) Structure–activity relationships of Pt/Al_2O_3 catalysts for CO and NO oxidation at diesel exhaust conditions. Appl Catal B Environ 126:315–325. doi:10.1016/j.apcatb.2012.07.029
6. Gracia FJ, Bollmann L, Wolf EE et al (2003) In situ FTIR, EXAFS, and activity studies of the effect of crystallite size on silica-supported Pt oxidation catalysts. J Catal 220:382–391. doi:10.1016/S0021-9517(03)00296-3
7. Szabó A, Henderson MA, Yates JT (1992) Oxidation of CO by oxygen on a stepped platinum surface: identification of the reaction site. J Chem Phys 96:6191–6202. doi:10.1063/1.462636
8. Yang J, Tschamber V, Habermacher D et al (2008) Effect of sintering on the catalytic activity of a Pt based catalyst for CO oxidation: experiments and modeling. Appl Catal B Environ 83:229–239. doi:10.1016/j.apcatb.2008.02.018
9. Auvray X, Pingel T, Olsson E, Olsson L (2013) The effect gas composition during thermal aging on the dispersion and NO oxidation activity over Pt/Al_2O_3 catalysts. Appl Catal B Environ 129:517–527. doi:10.1016/j.apcatb.2012.10.002
10. Irfan MF, Goo JH, Kim SD, Hong SC (2007) Effect of CO on NO oxidation over platinum based catalysts for hybrid fast SCR process. Chemosphere 66:54–59. doi:10.1016/j.chemosphere.2006.05.044
11. Hu L, Boateng KA, Hill JM (2006) Sol–gel synthesis of Pt/Al_2O_3 catalysts: effect of Pt precursor and calcination procedure on Pt dispersion. J Mol Catal Chem 259:51–60. doi:10.1016/j.molcata.2006.06.018
12. Reyes P, Oportus M, Pecchi G et al (1996) Influence of the nature of the platinum precursor on the surface properties and catalytic activity of alumina-supported catalysts. Catal Lett 37:193–197. doi:10.1007/BF00807753

13. Schmitz PJ, Kudla RJ, Drews AR et al (2006) NO oxidation over supported Pt: impact of precursor, support, loading, and processing conditions evaluated via high throughput experimentation. Appl Catal B Environ 67:246–256. doi:10.1016/j.apcatb.2006.05.012
14. McLean M, Mykura H (1966) The temperature dependence of the surface energy anisotropy of platinum. Surf Sci 5:466–481. doi:10.1016/0039-6028(66)90042-2
15. Cabié M, Giorgio S, Henry CR et al (2010) Direct observation of the reversible changes of the morphology of Pt nanoparticles under gas environment. J Phys Chem C 114:2160–2163. doi:10.1021/jp906721g
16. Yoshida H, Matsuura K, Kuwauchi Y et al (2011) Temperature-dependent change in shape of platinum nanoparticles supported on CeO 2 during catalytic reactions. Appl Phys Express 4:065001. doi:10.1143/APEX.4.065001
17. Hofmann G, Rochet A, Ogel E et al (2015) Aging of a Pt/Al_2O_3 exhaust gas catalyst monitored by quasi in situ X-ray micro computed tomography. RSC Adv 5:6893–6905. doi:10.1039/C4RA14007A
18. Simonsen SB, Chorkendorff I, Dahl S et al (2012) Effect of particle morphology on the ripening of supported Pt nanoparticles. J Phys Chem C 116:5646–5653. doi:10.1021/jp2098262
19. Aramendía MA, Benítez JA, Borau V et al (1999) Study of MgO and Pt/MgO systems by XRD, TPR, and ^{1} H MAS NMR. Langmuir 15:1192–1197. doi:10.1021/la9808972
20. Regalbuto JR, Navada A, Shadid S et al (1999) An experimental verification of the physical nature of Pt adsorption onto alumina. J Catal 184:335–348. doi:10.1006/jcat.1999.2471
21. Shelimov B, Lambert J-F, Che M, Didillon B (1999) Initial steps of the alumina-supported platinum catalyst preparation: a molecular study by ^{195}Pt NMR, UV–visible, EXAFS, and raman spectroscopy. J Catal 185:462–478. doi:10.1006/jcat.1999.2527
22. Oudenhuijzen MK, Kooyman PJ, Tappel B et al (2002) Understanding the influence of the pretreatment procedure on platinum particle size and particle-size distribution for SiO_2 impregnated with $[Pt^{2+}(NH_3)_4](NO_3^-)_2$: a combination of HRTEM, mass spectrometry, and quick EXAFS. J Catal 205:135–146. doi:10.1006/jcat.2001.3433
23. Mojet BL, Ramaker DE, Miller JT, Koningsberger DC (1999) Observation of a hydrogen-induced shape resonance on Pt/LTL catalysts and its relation with support acidity/alkalinity. Catal Lett 62:15–20. doi:10.1023/A:1019018215806
24. Gracia FJ, Miller JT, Kropf AJ, Wolf EE (2002) Kinetics, FTIR, and controlled atmosphere EXAFS study of the effect of chlorine on Pt-supported catalysts during oxidation reactions. J Catal 209:341–354. doi:10.1006/jcat.2002.3601
25. Gololobov AM, Bekk IE, Bragina GO et al (2009) Platinum nanoparticle size effect on specific catalytic activity in n-alkane deep oxidation: dependence on the chain length of the paraffin. Kinet Catal 50:830–836. doi:10.1134/S0023158409060068
26. Boorse R, Stark WJ, Mädler L et al (2003) Flame-made platinum/alumina: structural properties and catalytic behaviour in enantioselective hydrogenation. J Catal 213:296–304. doi:10.1016/S0021-9517(02)00082-9
27. Hannemann S, Grunwaldt J-D, Lienemann P et al (2007) Combination of flame synthesis and high-throughput experimentation: the preparation of alumina-supported noble metal particles and their application in the partial oxidation of methane. Appl Catal Gen 316:226–239. doi:10.1016/j.apcata.2006.09.034
28. Manasilp A, Gulari E (2002) Selective CO oxidation over Pt/alumina catalysts for fuel cell applications. Appl Catal B Environ 37:17–25. doi:10.1016/S0926-3373(01)00319-8
29. Li J, Hao J, Fu L et al (2004) Cooperation of Pt/Al_2O_3 and In/Al_2O_3 catalysts for NO reduction by propene in lean burn condition. Appl Catal Gen 265:43–52. doi:10.1016/j.apcata.2004.01.001
30. Djokić SS, Cavallotti PL (2010) Electroless deposition: theory and applications. In: Djokić SS (ed) Electrodeposition. Springer, New York, pp 251–289
31. Rao C, Trivedi D (2005) Chemical and electrochemical depositions of platinum group metals and their applications. Coord Chem Rev 249:613–631. doi:10.1016/j.ccr.2004.08.015
32. Leontyev I, Kuriganova A, Kudryavtsev Y et al (2012) New life of a forgotten method: electrochemical route toward highly efficient Pt/C catalysts for low-temperature fuel cells. Appl Catal Gen 431–432:120–125. doi:10.1016/j.apcata.2012.04.025
33. Smirnova NV, Kuriganova AB, Leont'eva DV et al (2013) Structural and electrocatalytic properties of Pt/C and Pt-Ni/C catalysts prepared by electrochemical dispersion. Kinet Catal 54:255–262. doi:10.1134/S0023158413020146
34. Boubnov A, Gänzler A, Conrad S et al (2013) Oscillatory CO oxidation over Pt/Al_2O_3 catalysts studied by in situ XAS and DRIFTS. Top Catal 56:333–338. doi:10.1007/s11244-013-9976-6
35. Karakaya C, Deutschmann O (2012) A simple method for CO chemisorption studies under continuous flow: adsorption and desorption behavior of Pt/Al_2O_3 catalysts. Appl Catal Gen 445–446:221–230. doi:10.1016/j.apcata.2012.08.022
36. Spenadel L, Boudart M (1960) Dispersion of platinum on supported catalysts. J Phys Chem 64:204–207. doi:10.1021/j100831a004
37. Grunwaldt J-D, van Vegten N, Baiker A (2007) Insight into the structure of supported palladium catalysts during the total oxidation of methane. Chem Commun 44:4635–4637. doi:10.1039/b710222d
38. Ravel B, Newville M (2005) ATHENA, ARTEMIS, HEPHAESTUS: data analysis for X-ray absorption spectroscopy using IFEFFIT. J Synchrotron Radiat 12:537–541. doi:10.1107/S0909049505012719
39. Rehr JJ, Albers RC (2000) Theoretical approaches to x-ray absorption fine structure. Rev Mod Phys 72:621–654. doi:10.1103/RevModPhys.72.621
40. Haneda M, Watanabe T, Kamiuchi N, Ozawa M (2013) Effect of platinum dispersion on the catalytic activity of Pt/Al_2O_3 for the oxidation of carbon monoxide and propene. Appl Catal B Environ 142–143:8–14. doi:10.1016/j.apcatb.2013.04.055
41. Siegel S, Hoekstra HR, Tani BS (1969) The crystal structure of beta-platinum dioxide. J Inorg Nucl Chem 31:3803–3807. doi:10.1016/0022-1902(69)80300-3
42. Zhou RS, Snyder RL (1991) Structures and transformation mechanisms of the η, γ and θ transition aluminas. Acta Crystallogr Sect B 47:617–630. doi:10.1107/S0108768191002719
43. Owen EA, Yates EL (1933) XLI. Precision measurements of crystal parameters. Lond Edinb Dublin Philos Mag J Sci 15:472–488. doi:10.1080/14786443309462199
44. Abid M, Paul-Boncour V, Touroude R (2006) Pt/CeO_2 catalysts in crotonaldehyde hydrogenation: selectivity, metal particle size and SMSI states. Appl Catal Gen 297:48–59. doi:10.1016/j.apcata.2005.08.048
45. Naresh D, Kumar VP, Harisekhar M et al (2014) Characterization and functionalities of Pd/hydrotalcite catalysts. Appl Surf Sci 314:199–207. doi:10.1016/j.apsusc.2014.06.156
46. Venderbosch RH, Prins W, van Swaaij WPM (1998) Platinum catalyzed oxidation of carbon monoxide as a model reaction in mass transfer measurements. Chem Eng Sci 53:3355–3366. doi:10.1016/S0009-2509(98)00151-1
47. Hauptmann W, Drochner A, Vogel H et al (2007) Global kinetic models for the oxidation of NO on platinum under lean conditions. Top Catal 42–43:157–160. doi:10.1007/s11244-007-0170-6
48. Matam SK, Kondratenko EV, Aguirre MH et al (2013) The impact of aging environment on the evolution of Al_2O_3 supported

Pt nanoparticles and their NO oxidation activity. Appl Catal B Environ 129:214–224. doi:10.1016/j.apcatb.2012.09.018
49. Putna ES, Vohs JM, Gorte RJ (1997) Oxygen desorption from α-Al_2O_3 (0001) supported Rh, Pt and Pd particles. Surf Sci 391:L1178–L1182. doi:10.1016/S0039-6028(97)00611-0
50. Oran U, Uner D (2004) Mechanisms of CO oxidation reaction and effect of chlorine ions on the CO oxidation reaction over Pt/CeO_2 and Pt/CeO_2/γ-Al_2O_3 catalysts. Appl Catal B Environ 54:183–191. doi:10.1016/j.apcatb.2004.06.011
51. Job N, Chatenet M, Berthon-Fabry S et al (2013) Efficient Pt/carbon electrocatalysts for proton exchange membrane fuel cells: avoid chloride-based Pt salts! J Power Sour 240:294–305. doi:10.1016/j.jpowsour.2013.03.188
52. Fogel S, Doronkin DE, Gabrielsson P, Dahl S (2012) Optimisation of Ag loading and alumina characteristics to give sulphur-tolerant Ag/Al_2O_3 catalyst for H_2-assisted NH_3-SCR of NOx. Appl Catal B Environ 125:457–464. doi:10.1016/j.apcatb.2012.06.014